Journal of The Electrochemical Society, **164** (2) G17-G22 (2017)
0013-4651/2017/164(2)/G17/6/$33.00 © The Electrochemical Society

Sensitive and Selective Electrochemical Biosensor Based on ELP-OPH/BSA/TiO_2NFs/AuNPs for Determination of Organophosphate Pesticides with *p*-Nitrophenyl Substituent

Jing Bao,[a] Changjun Hou,[a,z] Danqun Huo,[a] Qiuchen Dong,[b] Xiaoyu Ma,[b] Xiangcheng Sun,[b] Mei Yang,[a] Khaled Hussein Abd El Galil,[c] Wilfred Chen,[d] and Yu Lei[b,e,z]

[a]*Key Laboratory of Biorheological Science and Technology (Chongqing University), Ministry of Education, Bioengineering College, Chongqing University, Chongqing 400030, People's Republic of China*
[b]*Department of Biomedical Engineering, University of Connecticut, Storrs, Connecticut 06269, USA*
[c]*Department of Microbiology, Faculty of Pharmacy, Mansoura University, Mansoura, Egypt*
[d]*Department of Chemical and Biomolecular Engineering, University of Delaware, Newark, Delaware 19716, USA*
[e]*Department of Chemical and Biomolecular Engineering, University of Connecticut, Storrs, Connecticut 06269, USA*

We report herein a new electrochemical bisosensor based on elastin-like polypeptide-organophosphate hydrolase/bovine serum albumin/titanium oxide nanofibers/gold nanoparticles (ELP-OPH/BSA/TiO_2NFs/AuNPs) for highly sensitive and selective, rapid, one-step determination of organophosphate pesticides (OPs) with *p*-nitrophenyl substituent. ELP-OPH was purified from genetically engineered *Escherichia coli* (*E. coli*) taking the advantage of thermal-triggered phase-transition of ELP. The surface morphology and crystal structure of the as-prepared ELP-OPH/BSA/TiO_2NFs/AuNPs nanocomposites were characterized by scanning electron microscopy (SEM), transmission electron microscopy (TEM) and X-ray Diffraction (XRD), respectively. The electrochemical properties and catalytic behavior of the as-prepared electrodes for the determination of methyl parathion were systematically investigated using cyclic voltammetry (CV), differential pulse voltammetry (DPV) and amperometry (i–t). During OPs detection, OP compounds were selectively adsorbed to the TiO_2NFs surface due to the strong affinity of its phosphoric group with TiO_2NFs, while AuNPs were employed to provide a stable interface for promoting electron transfer between biomolecules and electrodes, thus enhanced sensing performance was accomplished. Under the optimized operating conditions, the as-prepared biosensor can detect methyl parathion with a wide dynamic ranges (up to 116.4 μM), a good sensitivity of 734 μA cm^{-2} mM^{-1} and the limit of detection (S/N = 3) as low as 29 nM. Its further application for determination of methyl parathion spiked into lake water samples was also demonstrated with an acceptable stability. All these features indicate that the as-developed ELP-OPH/BSA/TiO_2NFs/AuNPs/GCE holds great promise in rapid, sensitive, specific, and reliable detection of organophosphates pesticides.

Manuscript submitted May 12, 2016; revised manuscript received November 28, 2016. Published December 9, 2016.

Organophosphate compounds (OPs) are commercial pesticides and chemical warfare agents that can cause hazardous environmental effects and also neurological disorders in mankind.[1–4] Due to their high chemical stability in ambient conditions, they can maintain toxicity in water and/or soil for a long time, thus posing long-term environmental and health hazard.[5–9] Therefore, detection methods with advantages like fast response, low cost, high sensitivity, and high selectivity and reliability are highly desired for OPs determination. Previously, OPs measurement is available using conventional detection equipment, including gas or liquid chromatography, chemiluminescence, capillary electrophoresis, mass spectrometry and high-performance liquid chromatography.[10–15] However, the requirement of bulky and expensive instrumentations, and time-consuming sampling procedures limited their generalization for in-field application. In view of these problems, biosensors based on enzymes offer a good choice for being rapid, convenient, cost-effective, sensitive and accurate OPs detection.

Acetylcholinesterase (AChE) based biosensors have been extensively used to detect OPs based on the strong inhibition of AChE activity in the presence of OPs. Unfortunately, inhibition-type OPs biosensors usually suffer from interference from many toxic compounds like carbamate pesticides and toxic inhibitors, thus the selectivity of those sensors needs to be improved. Besides, a long incubation time is required to accomplish good irreversible inhibition reactions for better sensitivity.[16–19] On the contrary, the organophosphorus hydrolase (OPH) shows unique biocatalytic activity toward a wide range of OPs (e.g., paraoxon, parathion and methyl parathion, etc.), which makes it superior to AChE in OPs determination.[20–22] OPH takes *p*-nitrophenyl substituted OPs as substrates to generate electroactive *p*-nitrophenol (*p*-NP), which could result in a change in amperometric signal in real-time format.[23–25] In recent years, a few microbial biosensors with surface displayed OPH have been used for the detection of OPs. However, their sensitivity is relatively low probably due to the lower level of whole cell OPH activity.[26–28] OPH-based biosensors using purified enzyme have been proposed to analyze OPs, but the interminable and time-consuming process of enzyme purification has restricted its extensive application.[29–32] In this study, elastin-like polypeptide-organophosphate hydrolase (ELP-OPH) was purified from genetically engineered *Escherichia coli* (*E. coli*) based on the unique reversible inverse-phase transition of ELPs, which can greatly shorten the purification process of the OPH enzyme. In addition, the ELP domain could also improve long-term stability of the fusion enzyme.[33]

In addition to purified enzyme as a sensitive signaling element, the electrochemical performance of biosensors can be further improved using a plethora of nanomaterials.[34] Among those functional metal nanoparticles, gold nanoparticles (AuNPs) stand out as a good choice for their fascinating characteristics such as good optical properties, excellent electronic conduction, high catalytic efficiency and desirable biocompatibility.[35–37] Transition metal oxides like titanium oxide (TiO_2) and zirconium dioxide (ZrO_2) have also been studied for a number of biological and environmental applications including bioelectronics and antifouling materials owing to their non-toxicity, long-term stability, low cost, high catalytic activity and good biocompatibility.[38–40] In particular, TiO_2 has been employed for selectively trapping free OP compounds by virtue of its strong affinity to the phosphoric group in OPs.[41–44]

Herein, we presented the combination of TiO_2NFs/AuNPs nanocomposite and ELP-OPH to construct a new biosensor for rapid, selective and sensitive detection of organophosphate pesticides (see Scheme 1). To the best of our knowledge, this is the first report on OPH biosensor using TiO_2NFs/AuNPs nanohybrids, which could take the synergistic effects of individual components in nanocomposites to achieve high performance. Specifically, ELP-OPH was purified according to a phase-transition method, which is much faster and easier than other conventional enzyme purification methods. The as-prepared nanocomposite biosensor was systematically characterized using SEM, TEM and XRD. Cyclic voltammetry (CV), differential pulse voltammetry (DPV) and amperometry (i–t) was used to evaluate the electrochemical properties of the biosensor. The as-developed biosensor showed good selectivity, high sensitivity and acceptable stability, and could be applied for OPs monitoring in real samples.

[z]E-mail: houcj@cqu.edu.cn; yu.lei@uconn.edu

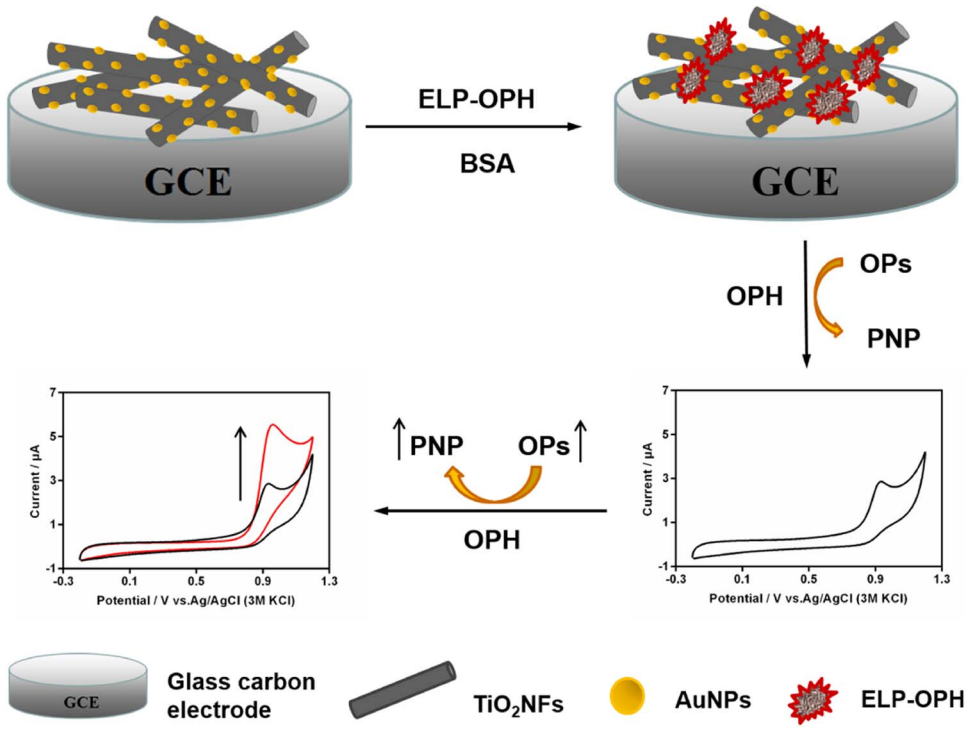

Scheme 1. Schematic representation of the construction of the as-prepared biosensor and its biosensing principle for OPs determination.

Experimental

Reagents and materials.—Genetically engineered *Escherichia coli* with ELP-OPH expression was employed to produce ELP-OPH.[33] Titanium isopropoxide ($Ti(OiPr)_4$, 97%), polyvinylpyrrolidone (PVP, MW = 1300000 g/mol), $HAuCl_4 \bullet 3H_2O$ (99.0%), Nafion 117 solution, and *N, N*-dimethylformamide (DMF, anhydrous, 99.8%) were purchased from Sigma-Aldrich. Methyl parathion was purchased from SUPELCO Analytical (USA) and used without further purification. Chitosan (CS) and bovine serum albumin (BSA) were purchased from Thermo Scientific and Bio-Rad (USA), respectively. Lake water samples were collected from the Hollow Lake (Mansfield, Connecticut, USA). All aqueous solutions were freshly prepared with deionized (DI) water (18 MΩ•cm) from Barnstead DI water system.

Preparation of ELP–OPH, TiO_2 NFs and AuNPs.—The ELP-OPH was purified from the cell culture according to a phase-transition method reported elsewhere.[33] Briefly, genetically engineered *Escherichia coli* with ELP-OPH (*ELP110-OPH-K6*) was incubated at 37°C with shaking, and the cell lysate was harvested through ultrasonication and centrifugation at 4°C. Next, 2 M NaCl was added to the cell lysate and the mixture was incubated at 37°C. Due to the phase transition of ELP, the resulting pellet containing ELP-OPH was recovered by centrifugation at 37°C. After re-dissolution of the pellet at 4°C, the supernatant was subject to an additional round of inverse temperature cycling, generating ELP-OPH with high purity.

Titanium oxide (TiO_2) nanofibers were synthesized according to the procedure reported elsewhere.[45] Briefly, titanium tetraisopropoxide ($Ti(OiPr)_4$, a sol–gel precursor to titania) was dissolved in poly(vinylpyrrolidone) (PVP) solution and electrospinning was conducted at an applied voltage of 20 kV to generate precursor composite nanofibers. Finally the TiO_2 nanofibers was generated after calcination of the composite nanofibers in air at 500°C for 3 h. 2 mg of TiO_2NFs were dispersed in 1 mL *N, N*-dimethylformamide (DMF), followed by 30-min sonication, to generate a homogenous suspension with a TiO_2 NFs concentration of 2 mg/mL.

To prepare AuNPs, all glassware used in the preparation was thoroughly cleaned in aqua regia (3 parts HCl, 1 part HNO_3), rinsed with ultrapure water, and oven-dried prior to use. Au colloid solutions were prepared according to a modified procedure from literature.[46] In brief, 50 mL of $HAuCl_4$ (0.015%) water solution was heated to boiling, and 2 mL of Na_3-citrate (1%) water solution was added. After 10-min boiling, the reaction flask was removed from oil bath, followed by additional 15-min stirring. The resulting solution of colloidal gold nanoparticles was characterized by the absorption at 521 nm. The as-prepared AuNPs water solution (14.68 nM) was stored at 4°C for future experiments.

Preparation of the ELP-OPH/BSA/TiO_2NFs/AuNPs modified electrodes.—Glassy carbon electrode (GCE, dia. 3 mm) was polished with 0.3 μm and 0.05 μm alumina slurries sequentially. After rinsed with DI water, the GCE was sonicated in acetone, ethanol and DI water, and then dried at room temperature. 6 μL of TiO_2NFs (2 mg/mL) and AuNPs suspensions (14.68 nM) with an appropriate volume ratio of TiO_2NFs and AuNPs was directly drop-cast onto the surface of GCE. Next, 10 μL of Nafion solution (0.05 wt%) was cast on the modified GCE to dry at room temperature. Highly porous Nafion membrane was then formed to entrap TiO_2NFs/AuNPs on the surface of the GCE. After drying in air, an aliquot of 8 μL ELP-OPH with 1% BSA (1/1, v/v) solution was coated on the prepared TiO_2NFs/AuNPs electrodes surface. Finally, 10 μL of Nafion solution (0.05 wt%) was loaded on the modified GCE to serve as the entrapping and protective layer to immobilize the ELP-OPH/BSA. The as-prepared electrode was denoted as ELP-OPH/BSA/TiO_2NFs/AuNPs/GCE. A similar procedure was also applied to prepare three control electrodes including ELP-OPH/BSA/GCE, ELP-OPH/BSA/AuNPs/GCE, and ELP-OPH/TiO_2 NFs/GCE.

Characterization and electrochemical measurements.—A JEOL 6335F field emission scanning electron microscopy (SEM) at an acceleration voltage of 10 kV and a transmission electron microscopy (TEM) (Zeiss LIBRA 200 FEG, 200kV) were employed to examine the morphology and the size of the as-prepared samples. The crystal structure of the samples was investigated by a D/Max 2500PC X-ray diffractometer (XRD). The final concentration of ELP-OPH solution was determined using a Cary 50 UV−vis spectrophotometer (Agilent

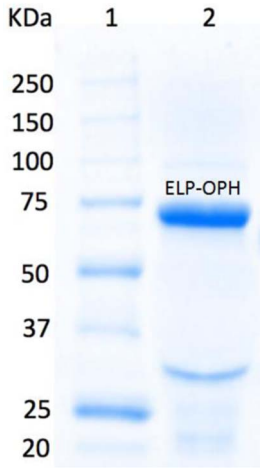

Figure 1. SDS-PAGE of elastin-like polypeptide organophosphate hydrolase (ELP-OPH) (lane 1: Protein standard; lane 2: purified ELP-OPH through two-cycle of centrifuge based on the phase-transition of ELP).

Technologies). Cyclic voltammetry (CV), differential pulse voltammetry (DPV) and amperometry (i–t) were carried out using a CHI 660D Electrochemical Workstation (CH Instrument, USA), while a silver/silver chloride (Ag/AgCl) and platinum (Pt) wire were used as the reference and auxiliary electrodes, respectively. The CVs were recorded by cycling the potential between −0.2 V and +1.2 V at a scan rate of 100 mV/s, while the DPV measurements were performed by applying a sweep potential from +0.4 V to +1.2 V with an amplitude of 100 mV and a pulse width of 0.25 s. All measurements were triplicated and recorded at room temperature.

Results and Discussion

Production and purification of ELP-OPH.—ELP-OPH was purified from genetically engineered *Escherichia coli* using ELP as the thermal-responsive purification tag through simple two-cycle of centrifuge. The purified ELP–OPH fusion protein (15 μL) was then analyzed on 10% SDS-PAGE gel (Figure 1). After two-cycle centrifuge based purification, ELP-OPH (MW of ∼ 60 kDa) with good purity was obtained (lane 2). The calculated ELP-OPH purity is ∼81% based on the band intensity analysis. The final concentration of ELP-OPH solution and the OPH activity (for methyl parathion) were determined to be 2.0 mg/mL and 3785 IU/mg through protein analysis and OPH activity assay, respectively.

Characterization of the as-prepared TiO_2NFs/AuNPs hybrid composite.—The micromorphology and the size distributions of the as-prepared nanomaterials were investigated using SEM and TEM. As shown in Figure 2A, the AuNPs exhibit homogeneous spherical shape and the average diameter of AuNPs is estimated to be 13 ± 2 nm (Figure 2A, inset). The TiO_2NFs display rod-shape and smooth surface with an average diameter of 100 nm (Figure 2B). The crystalline structures of the as-prepared AuNPs and TiO_2NFs were investigated by X-ray diffraction (XRD). As shown in Figures 2D and 2E, the diffraction peaks located at 2θ values of 38.10°, 44.16°, 64.40° and 77.38° correspond to (111), (200), (220) and (311) crystal planes of cubic structured Au, while the diffraction peaks located at 2θ values of 25.38°, 37.83°, 48.02°, 53.97°, 54.48°, 62.43°, 68.19°, 69.42°and 74.8° are assigned to (101), (004), (200), (105), (211), (204), (116), (220) and (215) crystal planes in TiO_2 nanofibers. Additionally, Figure 2C shows a typical SEM image of TiO_2NFs/AuNPs nanocomposite. The majority of AuNPs were uniformly decorated on the surface of the TiO_2NFs, while some of AuNPs were entrapped in the Nafion membrane. The elemental compositions (carbon, titanium, and gold) obtained from Energy Dispersive X-Ray Spectrometer (EDS) measurements (Inset of Figure 2C) clearly indicate the presence of both AuNPs and TiO_2NFs. All these results suggest the successful preparation of TiO_2NFs/AuNPs nanocomposite without losing their structure and properties. Such nanocomposite not only enhances the adsorption of OPs due to the strong affinity of TiO_2NFs to the phosphoric group in OPs, but also efficiently retains the bioactivity of OPH and promotes electron transfer during electrochemical detection.

Electrochemical behavior of methyl parathion at the as-prepared biosensors.—CV was first employed to investigate the electrochemical performances of the as-prepared biosensors in 0.05 M PBS buffer solution at the potential ranging from −0.2 V to +1.2 V (vs. Ag/AgCl). As shown in Figure 3A, an obvious peak can be observed at +0.93 V in the presence of 0.5 mM methyl parathion. It could be attributed to the electrochemical oxidation of the hydrolysis product (*p*-nitrophenol, *p*-NP), resulting from the hydrolysis of methyl parathion catalyzed by OPH. In addition, the oxidation current is proportional to the OP concentration.[47] In order to elucidate the role of each component in the biosensor, CVs of the electrodes modified with different material compositions were recorded in 0.05 M pH 7.4 PBS buffer solution containing 0.5 mM methyl parathion (Figure 3B). In contrast to the ELP-OPH/BSA/GCE (curve a), a much

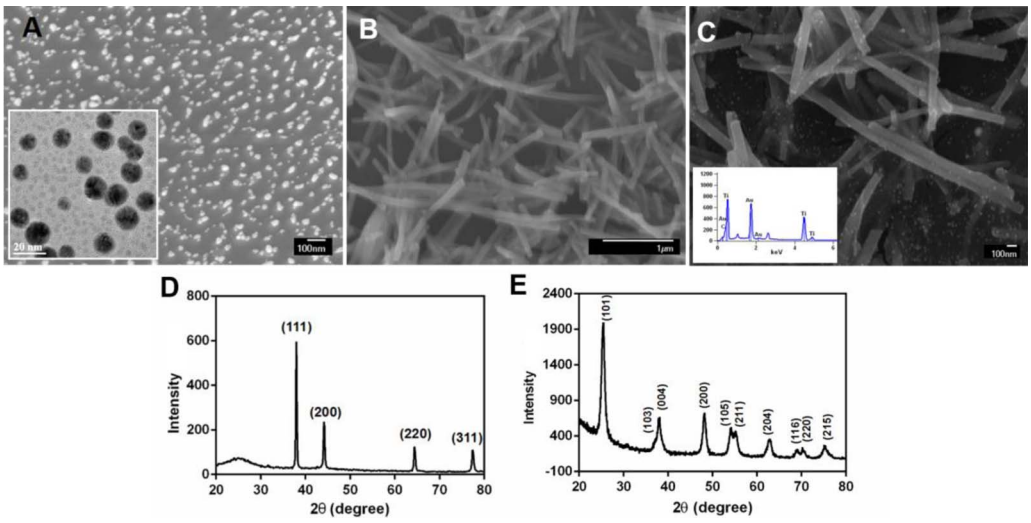

Figure 2. SEM images of AuNPs (A) (the inset is the TEM image); TiO_2NFs (B), and TiO_2NFs/AuNPs hybrid composite (C) (the inset is the EDS result); X-ray diffraction (XRD) patterns of AuNPs (D) and TiO_2NFs (E).

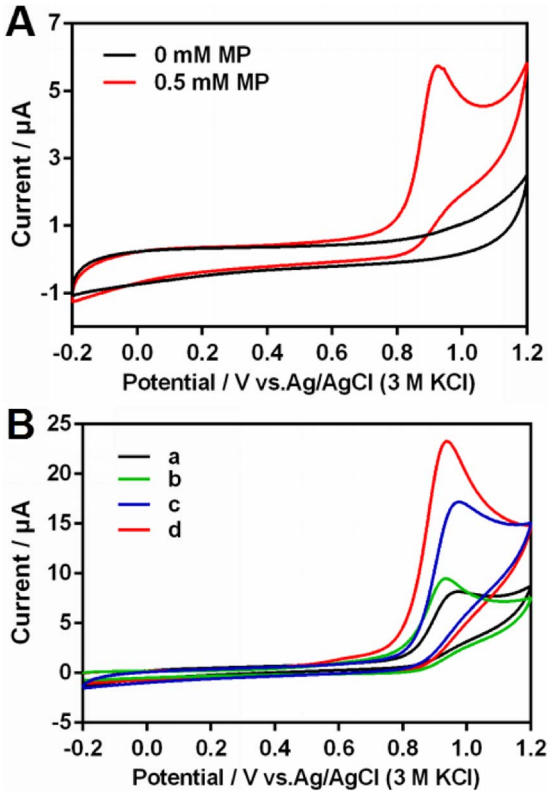

Figure 3. (A) CVs of the ELP-OPH/BSA/GCE in 0.05 M pH 7.4 PBS (a) and in 0.05 M pH 7.4 PBS containing 0.5 mM methyl parathion (b). (B) CVs of the different electrodes in 0.05 M pH 7.4 PBS containing 0.5 mM methyl parathion: (a) ELP-OPH/BSA/GCE, (b) ELP-OPH/BSA/TiO_2NFs/GCE, (c) ELP-OPH/BSA/AuNPs/GCE, and (d) ELP-OPH/BSA/TiO_2NFs/AuNPs/GCE. The scan rate is 100 mV/s.

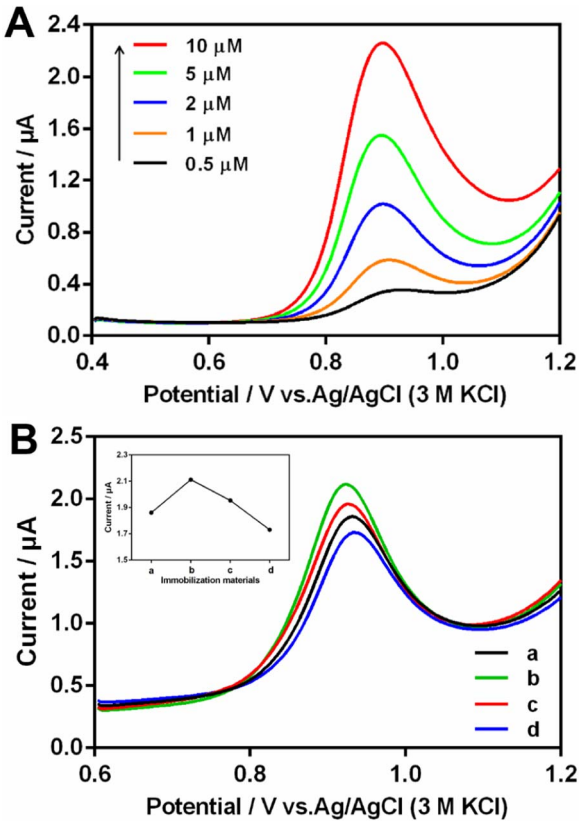

Figure 4. (A) DPVs on the ELP-OPH/BSA/TiO_2NFs/AuNPs/GCE in 0.05 M pH 7.4 PBS containing different concentrations of methyl parathion (from bottom to top, 0.5 μM, 1 μM, 2 μM, 5 μM, and 10 μM, respectively). (B) The effect of the entrapment material of biosensor on the response to 10 μM methyl parathion in 0.05 M pH 7.4 PBS: (a) ELP-OPH/TiO_2NFs/AuNPs/GCE, (b) ELP-OPH/BSA/TiO_2NFs/AuNPs/GCE, (c) ELP-OPH/NF/TiO_2NFs/AuNPs/GCE and (d) ELP-OPH/CS/TiO_2NFs/AuNPs/GCE, respectively. The inset shows the relationship between the response and the material used.

sharper peak was obtained at the ELP-OPH/BSA/TiO_2NFs/GCE (curve b). It was mainly attributed to the enhanced adsorption of OPs on TiO_2NFs. Furthermore, the oxidation peak current was significantly enhanced at the ELP-OPH/BSA/AuNPs/GCE (curve c), owing to enhanced electron transfer and good biocompatibility of AuNPs. Notably, the most prominent peak was observed at the ELP-OPH/BSA/TiO_2NFs/AuNPs/GCE (curve d), which was about five-fold higher than that of the ELP-OPH/BSA electrode. Such remarkable performance of the ELP-OPH/BSA/TiO_2NFs/AuNPs/GCE suggested that the TiO_2NFs/AuNPs nanocomposite can offer the enhanced adsorption of OPs, large surface area and excellent electronic conduction to improve the electrochemical performance of the as-developed biosensor.

The performance of the as-prepared biosensor for methyl parathion oxidation was further systematically studied using DPV. As shown in Figure 4A, the anodic differential pulse voltammetry of methyl parathion at the ELP-OPH/BSA/TiO_2NFs/AuNPs/GCE was recorded in 0.05 M pH 7.4 PBS buffer solution. The oxidation peak current at +0.93 V increased as methyl parathion concentration increased from 0.5 μM to 10 μM and methyl parathion as low as 500 nM can be easily detected using DPV on the ELP-OPH/BSA/TiO_2NFs/AuNPs/GCE. Such high sensitivity could be attributed to the synergistic effect of the enhanced adsorption of OPs, the enhanced electron transfer, and large surface area of nanomaterials.

Optimization of experimental conditions.—In order to improve the detection sensitivity of OPs at the ELP-OPH/BSA/TiO_2NFs/AuNPs/GCE, the effects of experimental conditions such as the material used to immobilize enzyme, the ratio of TiO_2NFs to AuNPs and the buffer pH on the biosensor response to OPs were systematically investigated. To optimize one parameter, all other parameters are maintained at their optimal conditions. Figure 4B shows the results of a study of the entrapment material used in the enzyme biosensor construction. Nafion (curve c) and chitosan (curve d) are widely used in the development of amperometric biosensors, while bovine serum albumin (curve b) is extensively employed to stabilize enzymes. Figure 4B shows that the current signal of the ELP-OPH/BSA/TiO_2NFs/AuNPs/GCE (curve b) is higher than the other control electrodes. Therefore, 1% BSA was used as entrapment material in the subsequent experiments. Furthermore, the ratio of TiO_2NFs to AuNPs in nanocomposite was optimized. The best normalized signal was obtained at 1:2 ratio (v/v) of TiO_2NFs/AuNPs, demonstrated in Figure 5A. The effect of the pH value on the performance of the biosensor is presented in Figure 5B. With the increasing buffer pH from 6.6 to 8.2, the normalized current signal increased initially, and then reached the maximum value at a pH of 7.4. Further increase of buffer pH resulted in a decline of the normalized signal. Thus, PBS buffer with at pH 7.4 was selected for subsequent experiments.

Amperometric detection of methyl parathion.—The ELP-OPH/BSA/TiO_2NFs/AuNPs/GCE was further applied for real-time amperometric detection of OPs at an operating potential of +0.93 V (vs. Ag/AgCl). Under the optimized operating conditions (Figure 6A), the oxidation current increased rapidly upon the successive continuous addition of methyl parathion from 0.1 μM to 20 μM every 50s (3 times per concentration) in a 5 mL 0.05 M pH 7.4 PBS buffer solution under stirring at 250 rpm. The response time is determined to be

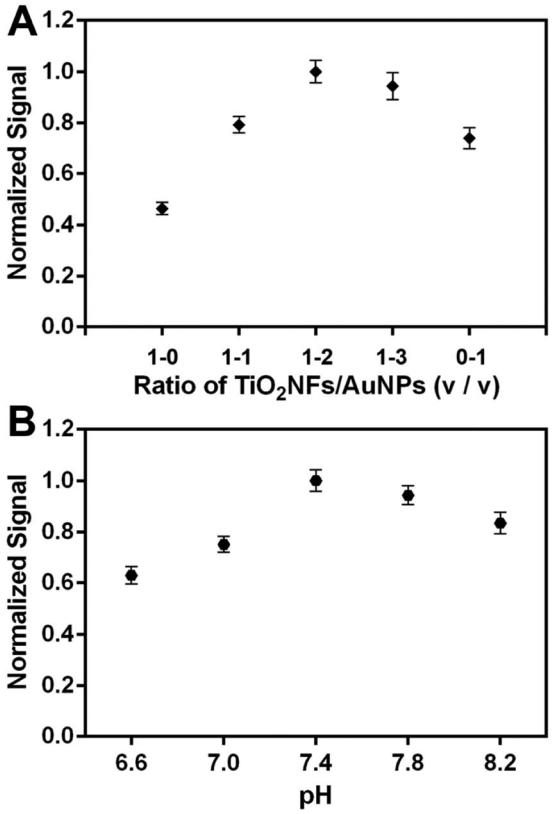

Figure 5. The effect of TiO_2NFs/AuNPs ratio (v/v) (A) and buffer pH (B) on the response of the ELP-OPH/BSA/TiO_2NFs/AuNPs /GCE to 10 μM methyl parathion in 0.05 M PH 7.4 PBS (all other parameters are operated under their optimal conditions). The response was normalized based on the response under optimized conditions.

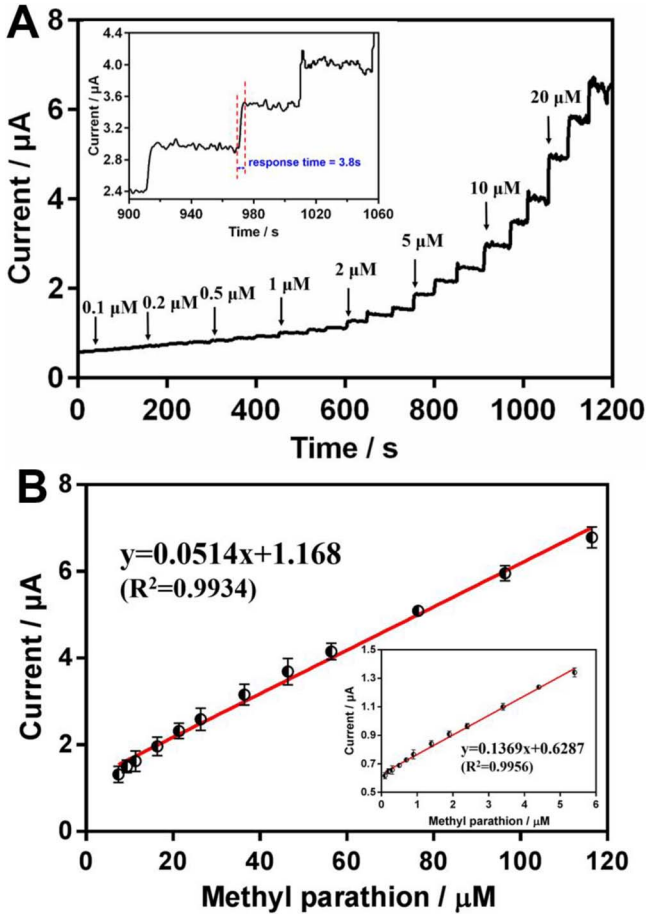

Figure 6. (A) Amperometric response of the ELP-OPH/BSA/TiO_2NFs/AuNPs/GCE toward continuous addition of methyl parathion from 0.1 μM to 20 μM in 0.05 M pH 7.4 PBS buffer (Inset shows the response time). **(B)** The corresponding calibration curve of the amperometric response to the concentration of methyl parathion from 5.4 μM to 116.4 μM (Inset shows the calibration curve for methyl parathion in the range of 0.1 μM to 5.4 μM).

around 3.8 s from the inset of Figure 6A indicating that the reaction on the developed electrode was very fast. The corresponding calibration plot for methyl parathion at the as-developed biosensor was presented in Figure 6B. An excellent sensitivity of 1955 μA cm^{-2} mM^{-1} is obtained in low OPs concentrations ranging from 0.1 μM to 5.4 μM (y (I) = 0.1369x + 0.6287, R^2 = 0.9956) in the inset of Figure 6B, while it decreases to 734 μA cm^{-2} mM^{-1} over a wide linear range from 5.4 μM to 116.4 μM (y (I) = 0.0514x + 1.168, R^2 = 0.9934). The calculated limit of detection (LOD) for methyl parathion is 29 nM (S/N = 3). Although methyl parathion was used as a *p*-nitrophenyl substituted OPs model in this study, parathion and paraoxon belonging to the same group can also be hydrolyzed to release *p*-NP by OPH with a higher catalytic rate compared to methyl parathion. Therefore, all of them can be detected sensitively.[28] Compared with other OPH-based biosensors for the detection of methyl parathion, such as spectrophotometric OPH-bacteria sensor[26] (linear ranges: 2.5∼200 μM; LOD: 1 μM), amperometric OPH/Nafion sensor[48] (linear ranges: up to 5 μM; LOD: 70 nM), OPH-bacteria sensor[49] (linear ranges: up to 140 μM; LOD: 20 nM), OPH/CNT sensor[50] (linear ranges: 2–10 μM; LOD: 0.8 μM), the present work shows a better or at least comparable sensing performance in terms of the detection limit and the dynamic detection range. This might be attributed to the synergistic effect of TiO_2NFs and AuNPs in the nanocomposite, which not only increases the absorption of OPs but also promotes the electrochemical oxidation and electron transfer between the electrode and catalyst. Moreover, the purification of ELP-OPH based on thermal-triggered phase transition of ELP was enabled in a simple and rapid purification process. Compared to the irreversible inhibition of AChE-based OPs biosensors, the as-developed OPH-based OPs biosensor using *p*-nitrophenyl substituted OPs as substrates, offers repeatable, cost-effective, and sensitive determination of OPs.

Reproducibility, stability study and application to real sample.— The reproducibility of the ELP-OPH/BSA/TiO_2NFs/AuNPs/GCE is another important parameter in evaluation of biosensor performance. The reproducibility was thus evaluated by DPV using 10 μM methyl parathion. The low relative standard deviation (RSD) of 3% (n = 3) demonstrates good reproducibility of the OPs biosensor. Moreover, the investigation on the long-term storage stability of as-prepared biosensor suggest no obvious decrease in the response to 5 μM methyl parathion for the first 7 days when stored in 0.05 M pH 7.4 PBS buffer at 4°C. After a 15-day period, the biosensor also retained 92% of its initial current signal to 5 μM methyl parathion, suggesting good stability for the developed biosensor. We lastly evaluated the feasibility of the sensor for practical applications using lake water spiked with methyl parathion as the simulated real sample. The lake water sample was first filtered through a well-defined 0.2 μm PVDF filter, and then its pH and ionic strength were adjusted to match the optimized buffer conditions. As shown in Table I, good recovery of spiked methyl

Table I. Recovery studies of spiked methyl parathion in lake water samples (each result was the average of five measurements).

Pesticides	Added (μM)	Found (μM)	Recovery (%)	RSD (%)
Methyl Parathion	0.50	0.52	104	4
	2.00	1.88	94	5

parathion (0.5 μM and 2 μM) in all lake water samples were obtained, ranging from 94 ± 5% to 104% ± 4. The results demonstrate that the as-developed OPs biosensor is potentially applicable for real sample measurement.

Conclusions

A ELP-OPH/BSA/TiO_2NFs/AuNPs biosensor for sensitive, selective and rapid detection of OPs with *p*-nitrophenyl substituent was successfully developed in the present study. Under the optimized operating conditions, the as-developed OPs biosensor showed excellent biosensing performance with a wide detection range, a fast response, and good stability. The limit of detection is as low as 29 nM for methyl parathion. The applicability of as-developed OPs biosensor for the spiked lake water samples demonstrated its good recovery rates. All these features indicate that the developed biosensor holds great promise in rapid, sensitive, repeatable, cost-effective and reliable detection of OPs.

Acknowledgment

This work was financially supported by the Natural Science Foundation of China (31171684), Chongqing's Postgraduate Research Innovation Projects (CYB16038), Key Technologies R&D Program of China (2014BAD07B02), Key Technologies R&D Program of Sichuan Province of China (2013FZ0043), Open Fund of Liquor-Making Biotech and Application Key Laboratory of Sichuan Province (NJ2014-03). We also thank the workstation in Sichuan ProvinceGY2015-01 and the supporting by sharing fund of Chongqing university's large equipment.

References

1. P. Kumar, K. Kim, and A. Deep, *Biosens. Bioeletron.*, **70**, 469 (2015).
2. M. Stoytcheva, R. Zlatev, V. Gochev, Z. Velkova, and G. Montero, *Anal. Methods*, **6**, 8232 (2014).
3. G. Mercey, T. Verdelet, J. Renou, M. Kliachyna, R. Baati, F. Nachon, L. Jean, and P. Renard, *Accounts of Chem. Res.*, **45**, 756 (2012).
4. A. Mulchandani, W. Chen, P. Mulchandani, J. Wang, and K. R. Rogers, *Biosens. Bioelectron.*, **16**, 225 (2001).
5. F. M. Raushel, *Curr. Opin. Microbiol.*, **5**, 288 (2002).
6. A. S. Allard and A. H. Neilson, *Int. Biodeter. Biodegr.*, **39**, 253 (1997).
7. B. K. Singh, *Nature Reviews Microbiology*, **7**, 156 (2009).
8. S. D. Aubert, Y. C. Li, and F. M. Raushel, *Biochemistry*, **43**, 5707 (2004).
9. H. Aleixo, A. A. Saczk, M. F. de Oliveira, and L. L. Okumura, *J. Electrochem. Soc.*, **159**, B775 (2012).
10. M. E. Sanchez, R. Mendez, X. Gomez, and J. Martin-Villacorta, *J. Liq. Chromatogr. R. T.*, **26**, 483 (2003).
11. I. A. T. Khan, Riazuddin, Z. Parveen, and M. Ahmed, *B. Environ. Contam. Tox.*, **79**, 454 (2007).
12. J. H. Lee, J. Y. Park, K. Min, H. J. Cha, S. S. Choi, and Y. J. Yoo, *Biosens. Bioelectron.*, **25**, 1566 (2010).
13. G. Erdogdu, *Journal of Analytical Chemistry*, **58**, 569 (2003).
14. A. Fidder, A. G. Hulst, D. Noort, R. de Ruiter, M. J. van der Schans, H. P. Benschop, and J. P. Langenberg, *Chemical Research in Toxicology*, **15**, 582 (2002).
15. H. Hu, X. Liu, F. Jiang, X. Yao, and X. Cui, *Chemistry Central Journal*, **4** (2010).
16. Q. Zhou, L. Yang, G. Wang, and Y. Yang, *Biosens. Bioelectron.*, **49**, 25 (2013).
17. A. Snyder, Z. Bo, Q. Sun, C. Martinez, and L. Stanciu, *J. Electrochem. Soc.*, **159**, B783 (2012).
18. Y. Ipek, H. Dincer, and A. Koca, *J. Electrochem. Soc.*, **161**, B183 (2014).
19. J. Bao, C. Hou, M. Chen, J. Li, D. Huo, M. Yang, X. Luo, and Y. Lei, *Journal of Agricultural and Food Chemistry*, **63**, 10319 (2015).
20. C. Karnati, H. Du, H. Ji, X. Xu, Y. Lvov, A. Mulchandani, P. Mulchandani, and W. Chen, *Biosens. Bioelectron*, **22**, 2636 (2007).
21. D. Du, W. Chen, W. Zhang, D. Liu, H. Li, and Y. Lin, *Biosens. Bioelectron*, **25**, 1370 (2010).
22. Y. Lei, P. Mulchandani, W. Chen, and A. Mulchandani, *Sensors-Basel*, **6**, 466 (2006).
23. S. H. Chough, A. Mulchandani, P. Mulchandani, W. Chen, J. Wang, and K. R. Rogers, *Electroanalysis*, **14**, 273 (2002).
24. A. Mulchandani, P. Mulchandani, S. Chauhan, I. Kaneva, and W. Chen, *Electroanalysis*, **10**, 733 (1998).
25. D. P. Dumas, S. R. Caldwell, J. R. Wild, and F. M. Raushel, *J. Biol. Chem.*, **264**, 19659 (1989).
26. X. Tang, B. Liang, T. Yi, G. Manco, I. Palchetti, and A. Liu, *Enzyme. Microb. Tech.*, **55**, 107 (2014).
27. Y. Lei, P. Mulchandani, W. Chen, J. Wang, and A. Mulchandani, *Biotechnol. Bioeng.*, **85**, 706 (2004).
28. X. Tang, T. Zhang, B. Liang, D. Han, L. Zeng, C. Zheng, T. Li, M. Wei, and A. Liu, *Biosens. Bioelectron.*, **60**, 137 (2014).
29. A. Mulchandani, P. Mulchandani, I. Kaneva, and W. Chen, *Analytical Chemistry*, **70**, 4140 (1998).
30. A. Mulchandani, I. Kaneva, and W. Chen, *Analytical Chemistry*, **70**, 5042 (1998).
31. A. Mulchandani and Rajesh, *Appl. Biochem. Biotech.*, **165**, 687 (2011).
32. Y. Lei, P. Mulchandani, J. Wang, W. Chen, and A. Mulchandani, *Environ. Sci. Technol.*, **39**, 8853 (2005).
33. M. Shimazu, A. Mulchandani, and W. Chen, *Biotechnol. Bioeng.*, **81**, 74 (2003).
34. J. Wang, *Small*, **1**, 1036 (2005).
35. M. C. Daniel and D. Astruc, *Chem. Rev.*, **104**, 293 (2004).
36. K. Saha, S. S. Agasti, C. Kim, X. Li, and V. M. Rotello, *Chem. Rev.*, **112**, 2739 (2012).
37. J. B. Jia, B. Q. Wang, A. G. Wu, G. J. Cheng, Z. Li, and S. J. Dong, *Analytical Chemistry*, **74**, 2217 (2002).
38. D. V. Bavykin, E. V. Milsom, F. Marken, D. H. Kim, D. H. Marsh, D. J. Riley, F. C. Walsh, K. H. El-Abiary, and A. A. Lapkin, *Electrochem. Commun.*, **7**, 1050 (2005).
39. J. Huang, X. Zhang, S. Liu, Q. Lin, X. He, X. Xing, W. Lian, and D. Tang, *Sensors and Actuators B: Chemical*, **152**, 292 (2011).
40. D. V. Bavykin, J. M. Friedrich, and F. C. Walsh, *Adv. Mater.*, **18**, 2807 (2006).
41. M. R. Larsen, T. E. Thingholm, O. N. Jensen, P. Roepstorff, and T. Jorgensen, *Mol. Cell. Proteomics*, **4**, 873 (2005).
42. Y. Yang, H. Tu, A. Zhang, D. Du, and Y. Lin, *Journal of Materials Chemistry*, **22**, 4977 (2012).
43. H. K. Kweon and K. Håkansson, *Analytical Chemistry*, **78**, 1743 (2006).
44. Y. Huang, Q. Zhou, J. Xiao, and G. Xie, *J. Sep. Sci.*, **33**, 2184 (2010).
45. Y. Ding, Y. Wang, L. Zhang, H. Zhang, C. M. Li, and Y. Lei, *Nanoscale*, **3**, 1149 (2011).
46. G. Frens, *Nature Physical Science*, **241**, 20 (1973).
47. A. Karami, A. M. Latifi, and S. Khodi, *J. Microbiol. Biotechn.*, **24**, 379 (2014).
48. A. Mulchandani, P. Mulchandani, W. Chen, J. Wang, and L. Chen, *Analytical Chemistry*, **71**, 2246 (1999).
49. P. Mulchandani, W. Chen, and A. Mulchandani, *Environ. Sci. Technol.*, **35**, 2562 (2001).
50. R. P. Deo, J. Wang, I. Block, A. Mulchandani, K. A. Joshi, M. Trojanowicz, F. Scholz, W. Chen, and Y. H. Lin, *Anal. Chim. ACTA*, **530**, 185 (2005).